



**HAL**  
open science

## Extraction of spin-averaged rovibrational transition frequencies in HD<sup>+</sup>

Jean-Philippe Karr, Jeroen C.J. Koelemeij

► **To cite this version:**

Jean-Philippe Karr, Jeroen C.J. Koelemeij. Extraction of spin-averaged rovibrational transition frequencies in HD<sup>+</sup>. 2023. hal-03927679

**HAL Id: hal-03927679**

**<https://hal.science/hal-03927679>**

Preprint submitted on 25 Feb 2023

**HAL** is a multi-disciplinary open access archive for the deposit and dissemination of scientific research documents, whether they are published or not. The documents may come from teaching and research institutions in France or abroad, or from public or private research centers.

L'archive ouverte pluridisciplinaire **HAL**, est destinée au dépôt et à la diffusion de documents scientifiques de niveau recherche, publiés ou non, émanant des établissements d'enseignement et de recherche français ou étrangers, des laboratoires publics ou privés.

# Extraction of spin-averaged rovibrational transition frequencies in $\text{HD}^+$ for the determination of fundamental constants

Jean-Philippe Karr\*

*Laboratoire Kastler Brossel, Sorbonne Université, CNRS, ENS-Université PSL,  
Collège de France, 4 place Jussieu, F-75005 Paris, France and  
Université d'Evry-Val d'Essonne, Université Paris-Saclay,  
Boulevard François Mitterrand, F-91000 Evry, France*

Jeroen C. J. Koelemeij†

*LaserLaB, Department of Physics and Astronomy, Vrije Universiteit Amsterdam,  
De Boelelaan 1081, 1081 HV Amsterdam, The Netherlands  
(Dated: December 23, 2022)*

We present a comprehensive analysis of all currently available high-accuracy frequency measurements of rotational and rovibrational transitions in the hydrogen molecular ion  $\text{HD}^+$ . Our analysis utilizes the theoretically calculated hyperfine structure to extract the values of three spin-averaged transition frequencies through a global linear least-squares adjustment that takes into account theory-induced correlations between the different transitions. We subsequently use the three spin-averaged transition frequencies as input data in a second adjustment which employs precise theoretical expressions for the transition frequencies, written as a function of the proton, deuteron and electron masses, the Rydberg constant, and the proton and deuteron charge radii. Our analysis shows that the  $\text{HD}^+$  data may significantly improve the value of the proton-electron mass ratio, in particular if combined with recent high-precision measurements of particle masses and mass ratios obtained from Penning traps.

## I. INTRODUCTION

Theoretical predictions of physical quantities are generally based on functional expressions that are derived from theoretical models such as quantum electrodynamics (QED). These expressions are parametrized in terms of fundamental physical constants, such as the electron relative atomic mass and the Rydberg constant. The fundamental constants themselves are determined from precision measurements, often performed on single particles or simple atomic quantum systems, by adjusting their values such that theoretical predictions match the experimental observations as closely as possible. Such adjustments, implemented via least-squares optimization of the constants of interest with respect to large bodies of input data, are carried out by standards organizations such as the Committee on Data for Science and Technology (CODATA) and the Atomic Mass Data Center (AMDC).

For example, the most precise determinations of the Rydberg constant,  $R_\infty$ , and the electric charge radii of the proton,  $r_p$ , and the deuteron,  $r_d$ , have been determined from laser spectroscopy of both electronic and muonic hydrogen and deuterium, complemented by high-precision QED theoretical predictions (see Ref. [1] and references therein). By contrast, the relative atomic masses of particles like the electron and light nuclei such as the proton and deuteron have traditionally been determined using Penning-trap experiments and (for the elec-

tron) theoretical calculations of bound-state  $g$ -factors; for recent examples see Refs. [2–7]. It was recognized already in 1976 by Wing et al. that vibrational spectroscopy of the hydrogen molecular ions, such as  $\text{H}_2^+$  and  $\text{HD}^+$ , could be used for alternative determinations of particle mass ratios provided that both the measurements and the theory of these three-body, two-center quantum systems would be sufficiently accurate [8]. This concept was extended to laser spectroscopy of antiprotonic helium,  $\bar{\text{p}}\text{He}$ , by Hori et al. who combined their results with precise *ab initio* theory for a meaningful determination of the antiproton-electron mass ratio which under the assumption of *CPT* invariance is equivalent to the proton-electron mass ratio,  $m_p/m_e$  [9–11]. As a result,  $\bar{\text{p}}\text{He}$  data were included in the 2006 and 2010 CODATA adjustments where they contributed primarily to the value of the electron relative atomic mass,  $A_r(\text{e})$  [12, 13]. However, the 2014 and 2018 CODATA adjustments no longer considered  $\bar{\text{p}}\text{He}$  after  $A_r(\text{e})$  was determined using Penning-trap measurements and QED theory with over one order of magnitude smaller uncertainty [2].

In the last two decades, intensive efforts have been devoted to laser spectroscopy of  $\text{HD}^+$  stored in radiofrequency (rf) ion traps. Pioneering experiments demonstrated trapping and sympathetic cooling of  $\text{HD}^+$  through co-trapped, laser-cooled beryllium ions [14], and subsequent spectroscopy [15, 16]. Similar approaches were implemented by other research groups [17, 18], leading to various demonstrations of spectroscopy at around the part-per-billion level [16, 19, 20], and determinations of the proton-electron mass ratio at a similar level of precision [20–22]. In recent years the accuracy of rotational and vibrational spectroscopy of  $\text{HD}^+$  was im-

\* karr@lkb.upmc.fr

† j.c.j.koelemeij@vu.nl

proved by nearly three orders of magnitude by use of techniques for Doppler-free excitation [23–25]. Meanwhile also the precision of theoretical (QED) predictions of relevant transition frequencies in  $\text{HD}^+$  was strongly improved to below the level of 10 parts per trillion (ppt), such that the uncertainty of theoretically predicted frequencies is now limited by (primarily) the uncertainty of the 2018 CODATA value of  $m_p/m_e$  [26–28]. As anticipated by Wing et al. [8] and more recently also by Karr et al. [29], the availability of theoretical and experimental transition frequencies with uncertainties in the low-ppt range enabled a determination of  $m_p/m_e$  with a precision of about 20 ppt [23–25]. These values represented not only the most precise determinations of  $m_p/m_e$  to date, but they also were found to be consistent with a precise measurement of the relative proton mass,  $A_r(\text{p})$ , that deviated significantly from other determinations of  $A_r(\text{p})$  that were included in the 2018 CODATA adjustment [1, 3, 4]. Furthermore it has been pointed out by several authors that results from  $\text{HD}^+$  and  $\bar{\text{p}}\text{He}$  are of interest as they form a linking pin between ‘atomic’ fundamental constants such as  $R_\infty$ ,  $r_p$  and  $r_d$ , and particle masses and mass ratios that are typically determined using Penning traps, while enabling cross checks of QED calculations of bound-state  $g$ -factors of the electron which are relevant to the determination of  $A_r(\text{e})$  [30, 31].

The recent advances in  $\text{HD}^+$  experiments and theory and their demonstrated potential for the determination of fundamental constants warrant a closer investigation of the further analysis required to prepare available  $\text{HD}^+$  data for a possible inclusion in future CODATA adjustments. One crucial issue here is that, in general, atomic and molecular spectroscopic data include line shifts due to hyperfine interactions, whereas CODATA adjustments have historically considered only energy differences between hyperfine centroids. This implies that experimental spectroscopic data must undergo a preparatory analysis in order to effectively remove the hyperfine shifts from the data. This also applies to the case of  $\text{HD}^+$ , and several methods have been developed to derive spin-averaged transition frequencies (i.e. the energy differences between the upper- and lower-state hyperfine centroids) from experimentally measured frequencies of groups of hyperfine components [23, 32]. Here it should be noted that in the absence of independent experimental data on the relevant  $\text{HD}^+$  hyperfine structure, the theoretically predicted hyperfine structure is used. We here adopt the approach of [32], which is based on a least-squares optimization and takes into account the effect of correlations between theoretical hyperfine coefficients.

This article is organized as follows. The state-of-the-art  $\text{HD}^+$  hyperfine theory used for the extraction of spin-averaged transition frequencies is reviewed in Sec. II, along with a discussion of correlated hyperfine theory errors. Section III summarizes the available experimental data (that include hyperfine shifts) related to three different rotational-vibrational transitions in  $\text{HD}^+$ , followed by a global adjustment of the three spin-averaged rotational-

vibrational transition frequencies in Sec. IV. In Sec V, the adjusted spin-averaged frequencies and their covariances are subsequently combined with theoretical expressions that are functional expressions of several fundamental constants of interest, including  $A_r(\text{p})$  and  $A_r(\text{e})$ , thus forming a set of  $\text{HD}^+$  observational equations. We use these in a second adjustment based on different sets of input data and observational equations (including e.g. also recent Penning-trap measurements), and present the values of  $m_p/m_e$  that can be derived from each adjustment to illustrate the potential improvement in the precision of this quantity enabled by  $\text{HD}^+$ . Conclusions are presented in Sec. VI

## II. STATUS OF HYPERFINE STRUCTURE THEORY

### A. Hyperfine Hamiltonian

The hyperfine structure of a given rovibrational state of  $\text{HD}^+$  can be described by the following effective spin Hamiltonian [33]:

$$\begin{aligned}
 H_{\text{eff}} = & E_1(\mathbf{L}\cdot\mathbf{s}_e) + E_2(\mathbf{L}\cdot\mathbf{I}_p) + E_3(\mathbf{L}\cdot\mathbf{I}_d) + E_4(\mathbf{I}_p\cdot\mathbf{s}_e) \\
 & + E_5(\mathbf{I}_d\cdot\mathbf{s}_e) + E_6\{2\mathbf{L}^2(\mathbf{I}_p\cdot\mathbf{s}_e) - 3[(\mathbf{L}\cdot\mathbf{I}_p)(\mathbf{L}\cdot\mathbf{s}_e) \\
 & + (\mathbf{L}\cdot\mathbf{s}_e)(\mathbf{L}\cdot\mathbf{I}_p)]\} + E_7\{2\mathbf{L}^2(\mathbf{I}_d\cdot\mathbf{s}_e) \\
 & - 3[(\mathbf{L}\cdot\mathbf{I}_d)(\mathbf{L}\cdot\mathbf{s}_e) + (\mathbf{L}\cdot\mathbf{s}_e)(\mathbf{L}\cdot\mathbf{I}_d)]\} \\
 & + E_8\{2\mathbf{L}^2(\mathbf{I}_p\cdot\mathbf{I}_d) - 3[(\mathbf{L}\cdot\mathbf{I}_p)(\mathbf{L}\cdot\mathbf{I}_d) + (\mathbf{L}\cdot\mathbf{I}_p)(\mathbf{L}\cdot\mathbf{I}_d)]\} \\
 & + E_9\{2\mathbf{L}^2\mathbf{I}_d^2 - \frac{3}{2}(\mathbf{L}\cdot\mathbf{I}_d) - 3(\mathbf{L}\cdot\mathbf{I}_d)^2\},
 \end{aligned} \tag{1}$$

where  $\mathbf{I}_d$ ,  $\mathbf{I}_p$ , and  $\mathbf{s}_e$  are the spins of the deuteron, proton, and electron, and  $\mathbf{L}$  the total angular momentum excluding electron and nuclear spins (denoted by  $\mathbf{N}$  in standard spectroscopic notation). The coefficients  $E_k$ ,  $k = 1, 2, \dots, 9$  depend on the rovibrational state ( $v, L$ ). This Hamiltonian includes all the spin-dependent interactions that appear at the leading order ( $m\alpha^4$ ), i.e. in the Breit-Pauli Hamiltonian, except for the proton-deuteron spin-spin contact interaction, which is negligibly small because of the strong Coulomb repulsion.

Additional spin-dependent interactions appear at higher orders ( $m\alpha^6$  and above). The largest missing term in Eq. (1) is a coupling between proton and deuteron ( $\mathbf{I}_p\cdot\mathbf{I}_d$ ) mediated by the electron. The coupling coefficient of this interaction was shown to be on the order of 100 Hz [34], which is much smaller than the theoretical uncertainty of  $E_4$  (see below). The above effective Hamiltonian may thus be considered as complete for our present purposes.

The largest terms in Eq. (1) are the electron-proton ( $E_4 \sim 900$  MHz in the vibrational ground state) and electron-deuteron ( $E_5 \sim 140$  MHz) spin-spin contact interactions. They were calculated with relative uncertainties below 1 ppm [35]. A key element allowing to

reach this high accuracy is that the total nuclear correction to  $E_4$  ( $E_5$ ) was determined from the difference between the experimental ground-state hyperfine splitting of the hydrogen (deuterium) atom and the corresponding nonrecoil QED prediction, under the assumption that the nuclear correction is entirely described by a contact (delta-function) term. Uncertainties associated with nuclear corrections are thus suppressed, and the theoretical precision is limited by yet unevaluated higher-order QED terms: (i) nonrecoil corrections, dominated by the contribution of relative order  $\alpha(Z\alpha^2)\ln(Z\alpha)$  [36, 37], and (ii) recoil corrections that deviate from the contact-term approximation, i.e. mainly the contribution of relative order  $(Z\alpha)^2(m/M)$  [38].

The next largest terms are the spin-orbit ( $E_1 \sim 30$  MHz in the vibrational ground state) and spin-spin tensor interactions ( $E_6 \sim 8$  MHz,  $E_7 \sim 1$  MHz for  $L = 1$ ). They were computed with few-ppm uncertainties through calculation of higher-order corrections at orders  $m\alpha^6$  [39] and  $m\alpha^7\ln(\alpha)$  [40, 41]. The uncertainty is dominated by yet unevaluated nonlogarithmic corrections at the  $m\alpha^7$  order.

The remaining hyperfine coefficients are much smaller, ranging from  $E_8 \sim 3$  kHz to  $E_2 \sim 30$  kHz. They were calculated in the framework of the Breit-Pauli Hamiltonian with account of the electron's anomalous magnetic moment [33]. In general, the expected relative accuracy of this approximation is on the order of  $\alpha^2$ , but in this case some second-order contributions induced by the leading hyperfine interaction terms can give larger contributions. Due to this, the relative uncertainty of  $E_2$ ,  $E_3$ , and  $E_8$  is estimated to  $5\alpha^2$  [41]. In the case of the  $E_9$  term that describes the effect of the deuteron quadrupole moment, second-order terms are too small to significantly influence the uncertainty. The relative uncertainty of  $E_9$  is estimated to 98 ppm [41], which accounts for both the theoretical uncertainty and the uncertainty of the deuteron quadrupole moment value from [42].

State-of-the art values of all the hyperfine coefficients, for ro-vibrational levels involved in published high-precision measurements, are given in Table I.

In the analysis of HD<sup>+</sup> experimental data, it is important to properly estimate correlations between theoretical errors  $\delta E_k(v, L)$  on these coefficients. As shown in [32], the assumed level of correlation can significantly influence the determination of spin-averaged frequencies of rovibrational transitions from an incomplete set of measurements of their hyperfine components. Here, we make assumptions similar to those presented in the Appendix C of [41] (see that reference for details):

- Perfect correlations are assumed between  $\delta E_4(v, L)$  and  $\delta E_4(v', L')$ , as well as between  $\delta E_5(v, L)$  and  $\delta E_5(v', L')$ .
- For the other hyperfine coefficients ( $k \neq 4, 5$ ), correlation coefficients between  $\delta E_k(v, L)$  and  $\delta E_k(v', L')$  are expected to be positive, but are difficult to estimate. In our analysis, we thus vary these

coefficients between 0 and 1 to investigate their influence on the spin-averaged frequencies and quantify the additional uncertainty associated with this indetermination, and quantify the mean shift and additional uncertainty associated with these correlations.

- Perfect correlations are assumed between  $\delta E_2(v, L)$  and  $\delta E_3(v, L)$ , as well as between  $\delta E_6(v, L)$  and  $\delta E_7(v, L)$ . This stems from the fact the the uncalculated QED terms causing theoretical uncertainties in both coefficients are of the same nature.
- The correlation coefficient between  $\delta E_4(v, L)$  and  $\delta E_5(v, L)$  is estimated to be  $r(E_4, E_5) = 0.4016$ .
- No other correlations are assumed between  $\delta E_k(v, L)$  and  $\delta E_l(v, L)$ .
- No correlations are assumed between  $\delta E_k(v, L)$  and  $\delta E_l(v', L')$  with  $k \neq l$  and  $(v, L) \neq (v', L')$ , except for those that are implied by the above hypotheses, e.g.:  $r(E_4(v, L), E_5(v', L')) = r(E_4, E_5) = 0.4016$ .

Except for the unknown correlation between  $\delta E_k(v, L)$  and  $\delta E_k(v', L')$  ( $k \neq 4, 5$ ), we do not consider the effect of uncertainties in other correlation coefficients. Indeed, although these uncertainties are not strictly zero, they are estimated to be too small to have any significant impact on the spin-averaged frequencies.

## B. Hyperfine splitting

The hyperfine structure of a rovibrational state  $(v, L)$  is obtained by diagonalizing the effective spin Hamiltonian (1). The adopted coupling scheme of angular momenta is [33]

$$\mathbf{F} = \mathbf{I}_p + \mathbf{s}_e, \quad \mathbf{S} = \mathbf{F} + \mathbf{I}_d, \quad \mathbf{J} = \mathbf{L} + \mathbf{S}. \quad (2)$$

The matrix elements of the effective spin Hamiltonian in the basis of coupled states  $|vLFSJ\rangle$  are calculated using standard angular algebra procedures.  $J$  is an exact quantum number, whereas  $F$  and  $S$  are only approximate quantum numbers. A spin eigenstate is denoted by  $|vL\tilde{F}\tilde{S}J\rangle$ , which is the state having the largest weight in its decomposition over the coupled basis states. In the following, we omit the  $\tilde{\sim}$  symbols for simplicity.

Since the matrix of  $H_{\text{eff}}$  is block diagonal with blocks of size  $4 \times 4$  at most, its eigenvalues  $E_{\text{hfs}}(v, L, F, S, J)$  can be expressed analytically as a function of the hyperfine interaction coefficients  $E_k$  (here it should be noted that the spin coefficients  $E_k$  are expressed in frequency units, whereas other energies, such as  $E_{\text{hfs}}$ , are in energy units). These expressions are then linearized around the theoretical values of the coefficients using the sensitivity coefficients

$$\gamma_k(v, L, F, S, J) = \frac{1}{h} \frac{\partial E_{\text{hfs}}(v, L, F, S, J)}{\partial E_k}. \quad (3)$$

The theoretical hyperfine shifts  $E_{\text{hfs}}$  and sensitivity coefficients  $\gamma_k$  of all the levels involved in the measurements to be analyzed, are given in Table II.

### III. AVAILABLE EXPERIMENTAL DATA

At the time of writing, ppt-range frequency measurements of three rotational-vibrational transitions in  $\text{HD}^+$  had been reported in peer-reviewed publications. These are the  $(v, L): (0, 0) \rightarrow (0, 1)$  rotational transition at 1.31 THz [23], the  $(v, L): (0, 0) \rightarrow (1, 1)$  rovibrational transition at 58.6 THz [25], and the  $(v, L): (0, 3) \rightarrow (9, 3)$  vibrational overtone at 415 THz [24]. All frequency measurements were made on  $\text{HD}^+$  ions stored in an rf trap, and sympathetically cooled to millikelvin temperatures via laser-cooled  $\text{Be}^+$  ions stored in the same trap. For further details on the experimental setups and the justification of the achieved measurement uncertainties we refer to the original publications.

Table III provides an overview of the frequencies (and their uncertainties) of the 10 measured hyperfine components belonging to the three rotational-vibrational transitions of interest. In all cases the experimental uncertainties receive appreciable contributions from statistical as well as systematic errors. In the uncertainty evaluation of the  $(v, L): (0, 0) \rightarrow (0, 1)$  and  $(v, L): (0, 0) \rightarrow (1, 1)$  transitions, no mention is made of possible correlated systematic errors [23, 25]. In the case of the  $(v, L): (0, 3) \rightarrow (9, 3)$  transition, a correlation between two negligibly small (sub-0.01-kHz) errors in the estimate of the Zeeman shift was identified [24]. In what follows we assume the errors of all experimental transition frequencies to be uncorrelated.

### IV. GLOBAL ADJUSTMENT OF SPIN-AVERAGED TRANSITION FREQUENCIES

#### A. Adjustment details

The spin-averaged transition frequencies are determined from a global linearized least-squares adjustment of the available theoretical and experimental data presented in Secs. II and III, respectively. We follow the fitting procedure described in the Appendix E of [43].

All the experimental data listed in Table III are included as input data for the adjustment. The associated ‘‘observational equations’’ (see [43] for details) read

$$\begin{aligned}
 & f[(v, L, a) \rightarrow (v', L', a')] \\
 & \doteq f_{\text{SA}}^{\text{exp}}[(v, L) \rightarrow (v', L')] + (E_{\text{hfs}}(v', L', a') - E_{\text{hfs}}(v, L, a)) / h \\
 & + \sum_{k=1}^9 (\gamma_k(v', L', a') \delta E_k(v', L') - \gamma_k(v, L, a) \delta E_k(v, L)),
 \end{aligned} \tag{4}$$

where the dotted equality sign means that the left and right hand sides are not equal in general (since the set of

equations is overdetermined) but should agree within estimated errors.  $a = (F, S, J)$  and  $a' = (F', S', J')$  are the initial and final hyperfine states,  $f_{\text{SA}}^{\text{exp}}[(v, L) \rightarrow (v', L')]$  is the spin-averaged frequency of the rovibrational transition, and  $\delta E_k(v, L)$  is an additive correction to the theoretical value of  $E_k(v, L)$  that is introduced to take theoretical uncertainties into account, as done in the CODATA adjustments [1].  $\delta E_k(v, L)$  is treated as an adjusted constant, and included as an input datum with zero value and an uncertainty equal to the theoretical uncertainty of  $E_k(v, L)$ . However, these data are partially redundant because some pairs of coefficients are perfectly correlated to each other as explained in Sec. II A. Redundant variables are eliminated using the relationships:

$$\delta E_k(v, L) = \delta E_k(0, 0) \frac{u_k(v, L)}{u_k(0, 0)}, \quad k = 4, 5, \tag{5a}$$

$$\delta E_l(v, L) = \delta E_k(v, L) \frac{u_l(v, L)}{u_k(v, L)}, \quad (k, l) = (2, 3) \text{ or } (6, 7). \tag{5b}$$

There is a total of  $N = 32$  input data: 10 experimental frequencies (Table III), and 22 additive energy corrections (Table IV). The total number of adjusted constants is  $M = 25$ : 3 spin-averaged transition frequencies and the 22 energy corrections.

#### B. Effect of unknown hyperfine correlation coefficients

As explained in Sec. II A, the level of correlation between some of the theoretical hyperfine coefficients (namely,  $E_k(v, L)$  and  $E_k(v', L')$  with  $k \neq 4, 5$ ) is not well known. We thus varied systematically their correlation coefficients between 0 and 1 to study their influence on spin-averaged frequencies. The latter were found to be mostly sensitive to the level of correlation between  $E_1(v, L)$  and  $E_1(v', L')$ , with a smaller effect from the correlation between  $E_6(v, L)$  (which itself is fully correlated with  $E_7(v, L)$ ) and  $E_6(v', L')$ . Similar correlations involving other coefficients ( $E_{2,3}$ ,  $E_8$ ,  $E_9$ ) have a negligible impact. In order to estimate the additional uncertainty and possible shift caused by the unknown correlation coefficients, we carried out a Monte-Carlo simulation similar to [32], as further detailed in the Appendix. We find that the mean shift of the simulated spin-averaged transition frequencies is well accounted for when carrying out a single adjustment using correlation coefficients of 0.5. Furthermore, we determine the full widths of the simulated frequency distributions to be 2.09 Hz, 144 Hz, and 237 Hz for the rotational,  $v = 0 \rightarrow 1$ , and  $v = 0 \rightarrow 9$  transitions, respectively. We define a conservative measure of the frequency uncertainty associated with the unknown correlation coefficients by taking the full width divided by two. As will be shown below, these correlation-induced uncertainties are much smaller than the frequency uncertainties resulting from the adjustment itself.

In addition, the correlation-induced shifts of the three spin-averaged transition frequencies are themselves either strongly correlated or strongly anticorrelated. This implies a correlation between the adjusted spin-averaged frequencies in addition to the correlations that may result from the adjustment itself. We construct the corresponding 'correlation-induced' correlation matrix by hand from the correlation-induced uncertainties defined above, and from the observation that for variations of a single hyperfine correlation coefficient, the resulting frequency shifts to the three adjusted spin-averaged frequencies are fully (anti)correlated (see also the Appendix).

### C. Results and discussion

The spin-averaged frequencies determined by the least-square adjustment described above are given in the second line of Table V.

The rotational transition is shifted by about four standard deviations with respect to the value of [23]. This is mainly due to the fact that we make different assumptions on correlations between theoretical errors, especially those between  $E_4(0,0)$  and  $E_4(0,1)$ . As justified in detail in Ref. [41], we assume perfect correlation, whereas zero correlation was assumed in the initial analysis [23]. The sensitivity of the rotational transition on the assumed level of correlation was already observed in [32] (see Fig 4 (b) in that reference). For the other transitions, the frequencies determined in this work are well within the error bars of the previous determinations.

The improvement of hyperfine structure theory [41] allows reducing the uncertainties of the  $v = 0 \rightarrow 1$  and  $v = 0 \rightarrow 9$  transition frequencies with respect to their initial determinations [24, 25]. For the rotational transition, the precision is only slightly improved, because in this case 6 spin components have been measured, making the extracted frequency much less sensitive to theoretical uncertainties.

The normalized residuals of the adjustment (assuming a value of 0.5 for the unknown correlation coefficients) are shown in Fig. 1. They reveal substantial discrepancies between the experimental data and the theoretical hyperfine structure:

- in three of the six components of the rotational transitions, labeled A1 ( $3.0\sigma$  or 121 Hz), A3 ( $2.1\sigma$  or 35 Hz), and A5 ( $-7.1\sigma$  or -427 Hz) (see labeling in Table III);
- in both components of the  $v = 0 \rightarrow 9$  transition, labeled A9 ( $-6.9\sigma$  or -4.5 kHz) and A10 ( $6.1\sigma$  or 3.6 kHz);
- in a few theoretical spin coefficients involved in the above two transitions, in particular  $E_1(v = 0, L = 1)$  ( $4.2\sigma$  or 484 Hz),  $E_6(v = 0, L = 1)$  ( $4.7\sigma$  or 85 Hz). Deviations slightly above  $2\sigma$  are also found in  $E_6(v = 1, L = 1)$ ,  $E_6(v = 0, L = 3)$ ,  $E_1(v = 9, L = 3)$ , and  $E_6(v = 9, L = 3)$ .

Discrepancies in the hyperfine structure of these two transitions had already been evidenced and discussed in previous works [35, 41]. Their origin is presently unknown; they could be due to a problem in the theory, in the experiment, or both.

We treat these deviations following the procedure used in the CODATA adjustments (see, e.g., [1]). A multiplicative expansion factor is applied to the initially assigned uncertainties of all (experimental and theoretical) input data, such that the absolute values of all normalized residuals are smaller than two. The required expansion factor is  $\eta = 3.56$ . As a result, the uncertainties of the spin-averaged frequencies are multiplied by the same factor (third line in Table V). The expanded uncertainties are one order of magnitude larger than the uncertainties associated with the unknown correlation coefficients.

The spin-averaged frequencies obtained by the least-squares adjustment have small but nonzero correlations between them due to the correlation between hyperfine theory errors  $\delta E_k$  in different rovibrational levels. The magnitude of the corresponding correlation coefficients is less than 0.01, and their values (and in some case also their signs) depend on the choice of hyperfine correlation coefficients (Sec. II A). Therefore, the correlations between the three adjusted spin-averaged transition frequencies have an uncertainty due to the unknown hyperfine theory correlations. In Sec. V we show that these correlations have a negligible impact on the fundamental constants that may be derived from the HD<sup>+</sup> data, and we do not investigate this particular source of uncertainty further here. However, for completeness we do combine the correlation matrix resulting from the adjustment with the correlation-induced correlation matrix that was constructed manually as described in Sec. IV B. The resulting (combined) uncertainties of the spin-averaged transition frequencies are listed in the last line of Table V, and their (combined) correlation coefficients are presented in Table VII.

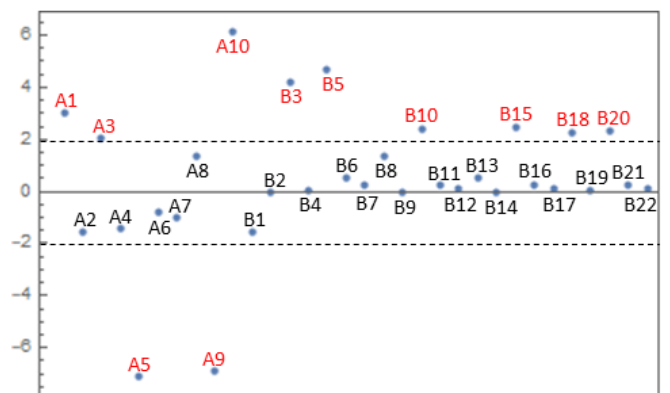


FIG. 1. Normalized residuals for the adjustment of spin-averaged transition frequencies.

## V. IMPLICATIONS FOR THE DETERMINATION OF PARTICLE MASSES

Using the spin-averaged frequencies determined in this work, we can now assess the potential contribution of HD<sup>+</sup> spectroscopy to the determination of the proton-electron mass ratio  $m_p/m_e$ . To do this, we use a least-squares adjustment following the same procedure as in the previous section, and compare three different scenarios:

- Adjustment 1 only includes Penning trap measurements related to the electron and proton atomic masses;
- Adjustment 2 only includes HD<sup>+</sup> spectroscopic data and values of fundamental constants involved in the theoretical energy levels of HD<sup>+</sup>;
- Adjustment 3 includes all input data of Adjustments 1 and 2.

### A. Adjustment details

Let us briefly describe Adjustment 1. It includes the 2018 CODATA value of electron mass, for which no new measurement has been reported since then. For the proton relative atomic mass, we use the value of  $A_r(^1\text{H})$  from the latest (2020) Atomic Mass Evaluation (AME) [44, 45], corrected for the electron mass and for the theoretical binding energy. This value takes into account recent high-precision Penning trap data [5, 6], except for a very precise measurement of the deuteron-to-proton mass ratio,  $m_d/m_p$ , performed in 2021 [7]. We thus also include the latter, together with the value of the deuteron mass deduced from the 2020 AME value of  $A_r(^2\text{H})$  (again corrected for the electron mass and the binding energy), which allows improving further the proton mass determination. Adjustment 1 thus comprises  $N = 4$  input data and  $M = 3$  adjusted parameters, the relative atomic masses of the electron, proton and deuteron ( $m_e, m_p, m_d$ ).

We now consider Adjustment 2. Theoretical rovibrational transition frequencies of HD<sup>+</sup> depend on the following fundamental constants:  $m_e, m_p, m_d$ , the Rydberg constant ( $R_\infty$ ), the charge radii of the proton ( $r_p$ ) and deuteron ( $r_d$ ), and the fine-structure constant ( $\alpha$ ). The dependence on  $\alpha$  is very weak because it only enters in the relativistic and QED corrections, and can be safely neglected without loss of precision. As noted in previous works, e.g., [23, 26]), the dependence on particle masses can to a good approximation be reduced to a dependence on a single parameter  $\mu_{pd}/m_e$ , where  $\mu_{pd}$  is the proton-deuteron reduced mass. HD<sup>+</sup> spectroscopic data can thus be used to constrain this quantity, as done in [23, 25]. However, from the perspective of a global adjustment of fundamental constants, it is not particularly

useful to introduce an additional parameter, and the simplest approach, which we will follow here, is to keep the particle masses ( $m_e, m_p, m_d$ ) as adjusted parameters, as done in the CODATA adjustment [1].

The theoretical expression of HD<sup>+</sup> transition frequencies as function of the fundamental constants ( $c_1 \equiv m_e, c_2 \equiv m_p, c_3 \equiv m_d, c_4 \equiv cR_\infty, c_5 \equiv r_p, c_6 \equiv r_d$ ) [26, 28, 46] is linearized around their 2018 CODATA values  $c_{i0}$ , so that each of the three spin-averaged frequencies determined in the previous section (inputs A1-A3 in Table VI) is associated with an observational equation of the form

$$f_{\text{SA}}^{\text{exp}}[(v, L) \rightarrow (v', L')] \doteq f_{\text{SA}}^{\text{theor}}[(v, L) \rightarrow (v', L')] + \delta E(v', L') - \delta E(v, L) + \sum_{i=1}^6 \beta_i(v, L, v', L')(c_i - c_{i0}), \quad (6)$$

where the theoretical transition frequency  $f_{\text{SA}}^{\text{theor}}[(v, L) \rightarrow (v', L')]$  is calculated with 2018 CODATA values of fundamental constants.  $\delta E(v, L)$  is an additive energy correction accounting for the theoretical uncertainty of the energy of the rovibrational state  $(v, L)$ , and  $\beta_i(v, L, v', L')$  is a sensitivity coefficient:

$$\beta_i(v, L, v', L') = \frac{\partial f_{\text{SA}}[(v, L) \rightarrow (v', L')]}{\partial c_i} \quad (7)$$

The theoretical frequencies and sensitivity coefficients are given in Table VIII. The frequencies differ very slightly from those given in [28] because they are calculated with 2018 CODATA values of  $m_e, m_p$  and  $m_d$ , whereas the values of [28] are obtained with 2018 CODATA values of  $m_p/m_e$  and  $m_d/m_e$ . Round-off errors in the published recommended values cause tiny shifts in the nonrelativistic energy levels. The sensitivity to the Rydberg constant is simply given by

$$\beta_4(v, L, v', L') = \frac{f_{\text{SA}}^{\text{theor}}[(v, L) \rightarrow (v', L')]}{cR_\infty}, \quad (8)$$

and the sensitivities to the nuclear radii are easily obtained by differentiating the expression of the total nuclear size correction [28, 46] with respect to  $r_p$  and  $r_d$ . Finally, the sensitivities to particle masses mainly originate from those of the nonrelativistic energy levels. Following the approach of [47], they can be expressed as

$$\beta_i(v, L, v', L') = \beta_i(v', L') - \beta_i(v, L), \quad (9a)$$

$$\beta_1(v, L) = -\frac{1}{2} \left( \frac{1}{m_p} + \frac{1}{m_d} \right) \langle \nabla_{\mathbf{R}}^2 \rangle - \frac{1}{2} \frac{1}{m_d} \langle \nabla_{\mathbf{r}_d}^2 \rangle - \frac{1}{m_d} \langle \nabla_{\mathbf{R}} \cdot \nabla_{\mathbf{r}_d} \rangle, \quad (9b)$$

$$\beta_2(v, L) = \frac{1}{2} \frac{m_e}{m_p^2} \langle \nabla_{\mathbf{R}}^2 \rangle, \quad (9c)$$

$$\beta_3(v, L) = \frac{m_e}{m_d^2} \left( \frac{1}{2} \langle \nabla_{\mathbf{R}}^2 \rangle + \frac{1}{2} \langle \nabla_{\mathbf{r}_d}^2 \rangle + \langle \nabla_{\mathbf{R}} \cdot \nabla_{\mathbf{r}_d} \rangle \right). \quad (9d)$$

Here,  $\mathbf{R}$  and  $\mathbf{r}_d$  are the respective positions of the proton and electron with respect to the deuteron. Brackets denote expectation values over the nonrelativistic wavefunction of the  $(v, L)$  rovibrational state, which are calculated numerically with high precision using variational wavefunctions [47].

Similarly to the hyperfine structure, theoretical uncertainties are accounted for by introducing additive corrections  $\delta E(v, L)$  to the theoretical energy level  $E(v, L)$ . They are treated as adjusted constants, and included as input data with zero value and an uncertainty equal to the theoretical uncertainty of  $E(v, L)$ . The theoretical uncertainties (B1-B5 in Table VI) and their correlation coefficients (see in Table VII) are estimated using the results of [28]. Correlation coefficients are found to be very close to 1, because the uncertainties are dominated by unevaluated QED terms, whereas numerical errors are negligibly small.

Since  $\text{HD}^+$  transition frequencies are mainly sensitive to a single combination of the three particle masses, i.e. the ratio  $\mu_{pd}/m_e$ , they cannot be used to constrain more than one mass parameter. Two independent mass inputs thus need to be included in the adjustment. We chose to include the 2018 CODATA value of the electron mass and the value of the deuteron mass deduced from the AME 2020 value of  $A_r(^2H)$  (C1-C2 in Table VI) in order to illustrate the potential respective contributions of  $\text{HD}^+$  spectroscopy and mass spectrometry data on the proton mass (C3-C4 in Table VI).

Finally, we also include the 2018 CODATA values of the other involved fundamental constants, i.e. the Rydberg constant and the proton and deuteron radii, in order to account for their uncertainties (C5-C7 in Table VI). The fine-structure constant is not included since its uncertainty has a negligibly small influence. In total, the Adjustment 2 contains  $N = 13$  input data and  $M = 11$  adjusted parameters: the fundamental constants  $c_i$ , with  $i = 1, \dots, 6$ , and the additive energy corrections for the five involved energy levels.

The Adjustment 3 gathers the input data of the first two adjustments, with  $N = 15$  input data and  $M = 11$  adjusted parameters.

## B. Results

The determinations of the proton-electron mass ratios from the three adjustments described above are shown in Table IX.

Adjustment 1 illustrates the potential precision of the proton-electron mass ratio permitted by Penning trap measurements alone. The recent measurement of  $m_d/m_p$  [7], combined with the AME 2020 value of  $m_d$ , allows the precision of the proton mass to be improved to  $8.2 \times 10^{-12}$  (not shown in Table IX). The relative uncertainty of the proton-electron mass ratio is then  $3.0 \times 10^{-11}$ , mainly limited by the electron mass.

Adjustment 2 provides an alternative determination

of  $m_p/m_e$ , where mass spectrometry data related to the proton is substituted by  $\text{HD}^+$  spectroscopic data. Its uncertainty is comparable to that of the first adjustment, and the obtained values are in reasonable agreement, with a mild ( $1.8\sigma$ ) tension. The  $\text{HD}^+$  result is in far better agreement with the AME 2020 value of the proton mass (here supplemented with recent  $m_d$  and  $m_d/m_p$  data) than with its previous (AME 2016) determination [48], which would yield  $m_p/ = 1\,836.152\,674\,00(18)$ .

The last adjustment (Adjustment 3) illustrates the potential improvement that can be obtained by combining Penning trap with  $\text{HD}^+$  spectroscopy data. Whereas the proton and deuteron masses are very precisely determined by mass spectrometry,  $\text{HD}^+$  spectroscopy, being sensitive to the nucleus-to-electron mass ratios, provides a link to the electron mass, allowing to improve the precision of  $m_e$  (not shown in Table IX) and  $m_p/m_e$  to  $1.8 \times 10^{-11}$ , which would represent an improvement by more than a factor of three over 2018 CODATA. It is worth noting that the adjustment reveals no significant tension in the data, all the normalized residuals being smaller than 1.2 in absolute value.

We carried out Adjustment 3 taking into account the weak correlations between the adjusted experimental spin-averaged frequencies, discussed in Sec. IV C. To assess the influence of these correlations, we repeated Adjustment 3 assuming zero correlation between the spin-averaged frequencies. The value of  $m_p/m_e$  obtained from this adjustment is identical to the one shown in line 3 of Table IX, indicating a negligible impact of these correlations on the determination of fundamental constants from recent  $\text{HD}^+$  theory and measurements.

## VI. CONCLUSION

In conclusion, we have carried out a comprehensive analysis of the available high-precision spectroscopic data of rotational and vibrational transitions in  $\text{HD}^+$ , with the aim of providing a set of spin-averaged rotational-vibrational transition frequencies that can serve as input data for future CODATA adjustments of the fundamental physical constants. A crucial part of the analysis involves the use of theoretically computed hyperfine structure to remove hyperfine shifts from the measured transition frequencies, taking into account correlated theory errors between the various rotational-vibrational levels involved. The experimental input data are complemented by the most recent theoretical predictions of the spin-averaged transition frequencies, and by linearized expressions that parametrize these theoretical predictions in terms of relevant fundamental constants. Uncertainties and correlation coefficients pertaining to the input data were also provided, which completes the set of observational equations and covariances needed for future CODATA adjustments. To illustrate the potential of the  $\text{HD}^+$  data, we have carried out adjustments of the electron, proton and deuteron relative atomic mass using state-of-the-art data



from Penning-trap measurements as well as the  $\text{HD}^+$  data presented here, using the resulting proton-electron mass ratio as a benchmark. We thus found that the  $\text{HD}^+$  data have a particularly large impact on the precision of the electron mass which, together with the precise values of the proton and deuteron masses from Penning-trap measurements, may improve the precision of  $m_p/m_e$  by more than a factor of three compared to the current 2018 CODATA value.

## ACKNOWLEDGMENTS

### Appendix: Monte-Carlo simulation

To assess the uncertainty associated with the unknown correlation coefficients  $r[E_k(v, L), E_k(v', L')] \equiv r_k$  (with  $k \neq 4, 5$ ) we carry out a Monte-Carlo simulation analogous to [32]. As explained in Sec. IV A, we set  $r_2 = r_3$  and  $r_6 = r_7$ . We subsequently choose random values from the interval  $[0, 1)$  for each of the coefficients of the vec-

tor  $(r_1, r_2, r_6, r_8, r_9)$ , and carry out the adjustment of the spin-averaged frequencies and the terms  $\delta E_k(v, L)$ . This is repeated 500 times, and in addition for the vectors  $(0, 0, 0, 0, 0)$  and  $(1 - \epsilon, 1 - \epsilon, 1 - \epsilon, 1 - \epsilon, 1 - \epsilon)$ , with  $\epsilon = 10^{-6}$  to avoid singular covariance matrices. Adjustments are carried out numerically using 100 digits of precision. Histograms of the Monte-Carlo distributions of adjusted transition frequencies are shown in Fig. A1. The full widths of the frequency distributions are 2.09 Hz, 144 Hz, and 237 Hz for the  $(v, L): (0, 0) \rightarrow (0, 1)$ ,  $(v, L): (0, 0) \rightarrow (1, 1)$  and  $(v, L): (0, 3) \rightarrow (9, 3)$  transitions, respectively; the deviation of the mean spin-averaged frequency from the frequency obtained for the  $(0.5, 0.5, 0.5, 0.5, 0.5)$  case is 0.05 Hz,  $-3$  Hz, and  $-2$  Hz (i.e. less than 3% of the full width). Figure A1 furthermore shows the dependence of the correlation-induced shift if all correlation coefficients are varied simultaneously. Comparing the shifts of the three transitions shows that the shift of the rotational transition is anticorrelated with the shift of the  $v = 0 \rightarrow 1$  and  $v = 0 \rightarrow 9$  transitions, whereas the shifts for the latter two are correlated.

- 
- [1] E. Tiesinga, P. J. Mohr, D. B. Newell, and B. N. Taylor, Codata recommended values of the fundamental physical constants: 2018, *Rev. Mod. Phys.* **93**, 025010 (2021).
- [2] S. Sturm, F. Köhler, J. Zatorski, A. Wagner, Z. Harman, G. Werth, W. Quint, C. H. Keitel, and K. Blaum, High-precision measurement of the atomic mass of the electron, *Nature* **506**, 467 (2014).
- [3] F. Heiße, F. Köhler-Langes, S. Rau, J. Hou, S. Junck, A. Kracke, A. Mooser, W. Quint, S. Ulmer, G. Werth, K. Blaum, and S. Sturm, High-precision measurement of the proton's atomic mass, *Phys. Rev. Lett.* **119**, 033001 (2017).
- [4] F. Heiße, S. Rau, F. Köhler-Langes, W. Quint, G. Werth, S. Sturm, and K. Blaum, High-precision mass spectrometer for light ions, *Phys. Rev. A* **100**, 022518 (2019).
- [5] S. Rau, F. Heiße, S. Köhler-Langes, F. Sasidharan, R. Haas, D. Renisch, C. E. Düllmann, W. Quint, S. Sturm, and K. Blaum, Penning trap mass measurements of the deuteron and the  $\text{HD}^+$  molecular ion, *Nature* **585**, 43 (2020).
- [6] D. J. Fink and E. G. Myers, Deuteron-to-proton mass ratio from the cyclotron frequency ratio of  $\text{H}_2^+$  to  $\text{D}^+$  with  $\text{H}_2^+$  in a resolved vibrational state, *Phys. Rev. Lett.* **124**, 013001 (2020).
- [7] D. J. Fink and E. G. Myers, Deuteron-to-proton mass ratio from simultaneous measurement of the cyclotron frequencies of  $\text{H}_2^+$  and  $\text{D}^+$ , *Phys. Rev. Lett.* **127**, 243001 (2021).
- [8] W. H. Wing, G. A. Ruff, W. E. Lamb, and J. J. Spezeski, Observation of the Infrared Spectrum of the Hydrogen Molecular Ion  $\text{HD}^+$ , *Phys. Rev. Lett.* **36**, 1488 (1976).
- [9] M. Hori, A. Dax, J. Eades, K. Gomikawa, R. S. Hayano, N. Ono, W. Pirkel, E. Widmann, H. A. Torii, B. Juhász, D. Barna, and D. Horváth, Determination of the antiproton-to-electron mass ratio by precision laser spectroscopy of  $\bar{p}\text{He}^+$ , *Phys. Rev. Lett.* **96**, 243401 (2006).
- [10] M. Hori, A. Sótér, D. Barna, A. Dax, R. Hayano, S. Friedreich, B. Juhász, T. Pask, E. Widmann, D. Horváth, L. Venturelli, and N. Zurlo, Two-photon laser spectroscopy of antiprotonic helium and the antiproton-to-electron mass ratio, *Nature* **475**, 484 (2011).
- [11] M. Hori, H. Aghai-Khozani, A. Sótér, D. Barna, A. Dax, R. Hayano, T. Kobayashi, Y. Murakami, K. Todoroki, H. Yamada, D. Horváth, and L. Venturelli, Buffer-gas cooling of antiprotonic helium to 1.5 to 1.7 K, and antiproton-to-electron mass ratio, *Science* **354**, 610 (2016).
- [12] P. J. Mohr, B. N. Taylor, and D. B. Newell, Codata recommended values of the fundamental physical constants: 2006, *Rev. Mod. Phys.* **80**, 633 (2008).
- [13] P. J. Mohr, B. N. Taylor, and D. B. Newell, Codata recommended values of the fundamental physical constants: 2010, *Rev. Mod. Phys.* **84**, 1527 (2012).
- [14] P. Blythe, B. Roth, U. Fröhlich, H. Wenz, and S. Schiller, Production of ultracold trapped molecular hydrogen ions, *Phys. Rev. Lett.* **95**, 183002 (2005).
- [15] B. Roth, J. C. J. Koelemeij, H. Daerr, and S. Schiller, Rovibrational spectroscopy of trapped molecular hydrogen ions at millikelvin temperatures, *Phys. Rev. A* **74**, 040501(R) (2006).
- [16] J. C. J. Koelemeij, B. Roth, A. Wicht, I. Ernsting, and S. Schiller, Vibrational spectroscopy of  $\text{HD}^+$  with 2-ppb accuracy, *Phys. Rev. Lett.* **98**, 173002 (2007).
- [17] J. C. J. Koelemeij, D. W. E. Noom, D. de Jong, M. A. Haddad, and W. Ubachs, Observation of the  $v' = 8 \leftarrow v = 0$  vibrational overtone in cold trapped  $\text{HD}^+$ , *Appl. Phys. B-Lasers Opt.* **107**, 1075 (2012).

- [18] J. Schmidt, T. Louvradoux, J. Heinrich, N. Sillitoe, M. Simpson, J.-P. Karr, and L. Hilico, Trapping, cooling, and photodissociation analysis of state-selected  $\text{H}_2^+$  ions produced by  $(3 + 1)$  multiphoton ionization, *Phys. Rev. Applied* **14**, 024053 (2020).
- [19] U. Bressel, A. Borodin, J. Shen, M. Hansen, I. Ernsting, and S. Schiller, Manipulation of Individual Hyperfine States in Cold Trapped Molecular Ions and Application to  $\text{HD}^+$  Frequency Metrology, *Phys. Rev. Lett.* **108**, 183003 (2012).
- [20] S. Alighanbari, M. G. Hansen, V. I. Korobov, and S. Schiller, Rotational spectroscopy of cold and trapped molecular ions in the Lamb-Dicke regime, *Nat. Phys.* **14**, 555 (2018).
- [21] J. Biesheuvel, J. -Ph. Karr, L. Hilico, K. S. E. Eikema, W. Ubachs, and J. C. J. Koelemeij, Probing QED and fundamental constants through laser spectroscopy of vibrational transitions in  $\text{HD}^+$ , *Nat. Commun.* **7**, 10385 (2016).
- [22] J. Biesheuvel, J. -Ph. Karr, L. Hilico, K. S. E. Eikema, W. Ubachs, and J. C. J. Koelemeij, High-precision spectroscopy of the  $\text{HD}^+$  molecule at the 1-p.p.b. level, *Appl. Phys. B-Lasers Opt.* **123**, 23 (2017).
- [23] S. Alighanbari, G. S. Giri, F. L. Constantin, V. I. Korobov, and S. Schiller, Precise test of quantum electrodynamics and determination of fundamental constants with  $\text{HD}^+$  ions, *Nature* **581**, 152 (2020).
- [24] S. Patra, M. Germann, J. -Ph. Karr, M. Haidar, L. Hilico, V. I. Korobov, F. M. J. Cozijn, K. S. E. Eikema, W. Ubachs, and J. C. J. Koelemeij, Proton-electron mass ratio from laser spectroscopy of  $\text{HD}^+$  at the part-per-trillion level, *Science* **369**, 1238 (2020).
- [25] I. V. Kortunov, S. Alighanbari, M. G. Hansen, G. S. Giri, V. I. Korobov, and S. Schiller, Proton-electron mass ratio by high-resolution optical spectroscopy of ion ensembles in the resolved-carrier regime, *Nat. Phys.* **17**, 569 (2021).
- [26] V. I. Korobov, L. Hilico, and J. -Ph. Karr, Fundamental transitions and ionization energies of the hydrogen molecular ions with few ppt uncertainty, *Phys. Rev. Lett.* **118**, 233001 (2017).
- [27] D. T. Aznabayev, A. K. Bekbaev, and V. I. Korobov, Leading-order relativistic corrections to the rovibrational spectrum of  $\text{H}_2^+$  and  $\text{HD}^+$  molecular ions, *Phys. Rev. A* **99**, 012501 (2019).
- [28] V. I. Korobov and J. -Ph. Karr, Rovibrational spin-averaged transitions in the hydrogen molecular ions, *Phys. Rev. A* **104**, 032806 (2021).
- [29] J. -Ph. Karr, L. Hilico, J. C. J. Koelemeij, and V. I. Korobov, Hydrogen molecular ions for improved determination of fundamental constants, *Phys. Rev. A* **94**, 050501(R) (2016).
- [30] S. G. Karshenboim and V. G. Ivanov, Quantum electrodynamics, high-resolution spectroscopy and fundamental constants, *Applied Physics B: Lasers and Optics* **123**, 18 (2017).
- [31] A. Antognini, S. Bacca, A. Fleischmann, L. Gastaldo, F. Hagelstein, P. Indelicato, A. Knecht, V. Lensky, B. Ohayon, V. Pascalutsa, N. Paul, R. Pohl, and F. Wauters, Muonic-Atom Spectroscopy and Impact on Nuclear Structure and Precision QED Theory. arXiv:2210.16929 [nucl-th] (2022).
- [32] J. C. J. Koelemeij, Effect of correlated hyperfine theory errors in the determination of rotational and vibrational transition frequencies in  $\text{HD}^+$ , *Molecular Physics*, e2058637 (2022), <https://doi.org/10.1080/00268976.2022.2058637>.
- [33] D. Bakalov, V. I. Korobov, and S. Schiller, High-precision calculation of the hyperfine structure of the  $\text{HD}^+$  ion, *Phys. Rev. Lett.* **97**, 243001 (2006).
- [34] V. I. Korobov, Precision spectroscopy of the hydrogen molecular ions: present status of theory and experiment, *Phys. Part. Nucl.* **53**, 787 (2022).
- [35] J. -Ph. Karr, M. Haidar, L. Hilico, Z.-X. Zhong, and V. I. Korobov, Higher-order corrections to spin-spin scalar interactions in  $\text{HD}^+$  and  $\text{H}_2^+$ , *Phys. Rev. A* **102**, 052827 (2020).
- [36] A. Layzer, New logarithmic radiative corrections to the hyperfine splitting in hydrogenic atoms, *Nuovo Cim.* **33**, 1538 (1964).
- [37] D. E. Zwanziger, Radiative corrections to hyperfine structure in hydrogen, *Nuovo Cim.* **34**, 77 (1964).
- [38] G. T. Bodwin and D. R. Yennie, Some recoil corrections to the hydrogen hyperfine splitting, *Phys. Rev. D* **37**, 498 (1988).
- [39] V. I. Korobov, J.-P. Karr, M. Haidar, and Z.-X. Zhong, Hyperfine structure in the  $\text{H}_2^+$  and  $\text{HD}^+$  molecular ions at order  $m\alpha^6$ , *Phys. Rev. A* **102**, 022804 (2020).
- [40] M. Haidar, V. I. Korobov, L. Hilico, and J.-P. Karr, Higher-order corrections to spin-orbit and spin-spin tensor interactions in hydrogen molecular ions: theory and application to  $\text{H}_2^+$ , *Phys. Rev. A* **106**, 022816 (2022).
- [41] M. Haidar, V. I. Korobov, L. Hilico, and J.-P. Karr, Higher-order corrections to the spin-orbit and spin-spin tensor interactions in  $\text{HD}^+$ , *Phys. Rev. A* **106**, 042815 (2022).
- [42] M. Puchalski, J. Komasa, and K. Pachucki, Hyperfine structure of the first rotational level in  $\text{H}_2$ ,  $\text{D}_2$  and  $\text{HD}$  molecules and the deuteron quadrupole moment, *Phys. Rev. Lett.* **125** (2020).
- [43] P. J. Mohr and B. N. Taylor, CODATA recommended values of the fundamental physical constants: 1998, *Rev. Mod. Phys.* **72**, 351 (2000).
- [44] M. Wang, W. J. Huang, F. G. Kondev, G. Audi, and S. Naimi, The AME 2020 atomic mass evaluation (II). Tables, graphs and references. Available: <https://www-nds.iaea.org/amdc/>, *Chin. Phys. C* **45**, 030003 (2021).
- [45] W. J. Huang, M. Wang, F. G. Kondev, G. Audi, and S. Naimi, The AME 2020 atomic mass evaluation (I). Evaluation of input data, and adjustment procedures, *Chin. Phys. C* **45**, 030002 (2021).
- [46] V. I. Korobov, Leading-order relativistic and radiative corrections to the rovibrational spectrum of  $\text{H}_2^+$  and  $\text{HD}^+$  molecular ions, *Phys. Rev. A* **74**, 052506 (2006).
- [47] S. Schiller and V. Korobov, Tests of time independence of the electron and nuclear masses with ultracold molecules, *Phys. Rev. A* **71**, 032505 (2005).
- [48] M. Wang, G. Audi, F. G. Kondev, W. Huang, S. Naimi, and X. Xu, The AME2016 atomic mass evaluation (II). Tables, graphs and references, *Chin. Phys. C* **41**, 030003 (2017).

$(v, L)$	$E_1$	$E_2$	$E_3$	$E_4$	$E_5$	$E_6$	$E_7$	$E_8$	$E_9$
(0, 0)				925 394.159(860)	142 287.556(84)				
(0, 1)	31 985.417(116)	-31.345(8)	-4.809(1)	924 567.718(859)	142 160.670(84)	8611.299(18)	1321.796(3)	-3.057(1)	5.660(1)
(1, 1)	30 280.736(109)	-30.463(8)	-4.664(1)	903 366.501(839)	138 910.266(82)	8136.858(17)	1248.963(3)	-2.945(1)	5.653(1)
(0, 3)	31 628.097(114)	-30.832(8)	-4.733(1)	920 479.981(855)	141 533.075(83)	948.542(2)	145.597	-0.335	0.613
(9, 3)	18 270.853(62)	-21.304(6)	-3.225(1)	775 706.122(721)	119 431.933(73)	538.999(1)	82.726	-0.219	0.501

TABLE I. Theoretical hyperfine coefficients of rovibrational states of HD<sup>+</sup> involved in high-precision measurements, in kHz. The values of  $E_4$ ,  $E_5$  ( $E_1$ ,  $E_6$ ,  $E_7$ ) were calculated in Ref. [35] (Ref. [41]). Those of  $E_2$ ,  $E_3$ ,  $E_8$ ,  $E_9$  are taken from [33]. The value of  $E_9$  has been updated using the latest determination of the deuteron's quadrupole moment [42].

$(v, L)$	$(F, S, J)$	$E_{\text{hfs}}/h$ (kHz)	$\gamma_1$	$\gamma_2$	$\gamma_3$	$\gamma_4$	$\gamma_5$	$\gamma_6$	$\gamma_7$	$\gamma_8$	$\gamma_9$
(0, 0)	(0, 1, 1)	-705 735.655(639)				-0.7367	-0.1688				
	(1, 0, 0)	89 060.984(197)				0.2500	-1.0000				
	(1, 1, 1)	171 894.797(194)				0.2367	-0.3312				
	(1, 2, 2)	302 492.318(235)				0.2500	0.5000				
(0, 1)	(0, 1, 2)	-707 870.694(637)	-0.1070	0.1110	0.9953	-0.7338	-0.1845	0.0100	0.1434	-0.1572	-0.4930
	(1, 0, 1)	79 986.308(204)	-0.4286	-0.3861	0.6539	0.2494	-0.9084	-1.0279	0.8343	0.7206	-0.5019
	(1, 1, 2)	183 682.795(196)	0.3319	0.1539	0.5142	0.2341	-0.3152	0.2555	-0.5821	-0.4019	0.2287
	(1, 2, 1)	269 283.177(241)	-0.5693	-0.5592	-1.7183	0.2500	0.4251	0.0392	-3.3471	-3.2839	-2.9444
	(1, 2, 3)	312 567.273(242)	0.5000	0.5000	1.0000	0.2500	0.5000	-0.5000	-1.0000	-1.0000	-0.5000
	(1, 2, 2)	314 228.466(238)	-0.2249	-0.2649	-0.5096	0.2497	0.4997	1.7345	3.4387	3.5591	1.7643
(1, 1)	(1, 2, 1)	263 806.300(235)	-0.5753	-0.5654	-1.7152	0.2500	0.4296	-0.0105	-3.3687	-3.3063	-2.9087
	(1, 2, 3)	305 099.957(236)	0.5000	0.5000	1.0000	0.2500	0.5000	-0.5000	-1.0000	-1.0000	-0.5000
(0, 3)	(0, 1, 4)	-711 832.144(631)	-0.4142	0.4242	2.9867	-0.7267	-0.2156	0.2750	3.0796	-3.3289	-7.4000
	(1, 2, 5)	338 970.635(290)	1.5000	1.5000	3.0000	0.2500	0.5000	-7.5000	-15.0000	-15.0000	-7.5000
(9, 3)	(0, 1, 4)	-596 833.613(533)	-0.3590	0.3727	2.9847	-0.7303	-0.2017	0.1934	2.4743	-2.7221	-7.3853
	(1, 2, 5)	275 723.281(219)	1.5000	1.5000	3.0000	0.2500	0.5000	-7.5000	-15.0000	-15.0000	-7.5000

TABLE II. Theoretical hyperfine shifts (column 3) and sensitivity coefficients (columns 4-12) for all the levels involved in high-precision measurements. The uncertainties of the hyperfine shifts are calculated assuming no correlation between  $\delta E_k(v, L)$  and  $\delta E_k(v', L')$  for  $k \neq 4, 5$ , which provides an upper bound of the uncertainty.

$(v, L) \rightarrow (v', L')$	Label	$(F, S, J)$	$(F', S', J')$	Value (kHz)	Alt. label	Ref.
(0, 0) $\rightarrow$ (0, 1)	A1	(1, 2, 2)	(1, 2, 1)	1,314,892,544.276(40)	12	[23]
	A2	(1, 0, 0)	(1, 0, 1)	1,314,916,678.487(64)	14	
	A3	(0, 1, 1)	(0, 1, 2)	1,314,923,618.028(17)	16	
	A4	(1, 2, 2)	(1, 2, 3)	1,314,935,827.695(37)	19	
	A5	(1, 2, 2)	(1, 2, 2)	1,314,937,488.614(60)	20	
	A6	(1, 1, 1)	(1, 1, 2)	1,314,937,540.762(46)	21	
(0, 0) $\rightarrow$ (1, 1)	A7	(1, 2, 2)	(1, 2, 1)	58,605,013,478.03(19)	12	[25]
	A8	(1, 2, 2)	(1, 2, 3)	58,605,054,772.08(26)	16	
(0, 3) $\rightarrow$ (9, 3)	A9	(0, 1, 4)	(0, 1, 4)	415,265,040,503.57(59)	$F = 0$	[24]
	A10	(1, 2, 5)	(1, 2, 5)	415,264,862,249.16(66)	$F = 1$	

TABLE III. Experimentally determined transition frequencies of various hyperfine components used in the adjustment of the spin-averaged transition frequencies (Sec. IV). The alternate labels for the hyperfine components in column 6 are those used in the original references (column 7).

	Input datum	Value (kHz)		Input datum	Value (kHz)
B1	$\delta E_4(0, 0)$	0.000(860)	B12	$\delta E_9(1, 1)$	0.000 00(55)
B2	$\delta E_5(0, 0)$	0.000(84)	B13	$\delta E_1(0, 3)$	0.000(114)
B3	$\delta E_1(0, 1)$	0.000(116)	B14	$\delta E_2(0, 3)$	0.0000(82)
B4	$\delta E_2(0, 1)$	0.0000(83)	B15	$\delta E_6(0, 3)$	0.0000(20)
B5	$\delta E_6(0, 1)$	0.000(18)	B16	$\delta E_8(0, 3)$	0.000 000(89)
B6	$\delta E_8(0, 1)$	0.000 00(81)	B17	$\delta E_9(0, 3)$	0.000 000(60)
B7	$\delta E_9(0, 1)$	0.000 00(55)	B18	$\delta E_1(9, 3)$	0.000(62)
B8	$\delta E_1(1, 1)$	0.000(109)	B19	$\delta E_2(9, 3)$	0.0000(57)
B9	$\delta E_2(1, 1)$	0.0000(81)	B20	$\delta E_6(9, 3)$	0.0000(12)
B10	$\delta E_6(1, 1)$	0.000(17)	B21	$\delta E_8(9, 3)$	0.000 000(58)
B11	$\delta E_8(1, 1)$	0.000 00(78)	B22	$\delta E_9(9, 3)$	0.000 000(49)

TABLE IV. Input data for the additive energy corrections to account to the theoretical uncertainties of hyperfine interaction coefficients.

	(0, 0) $\rightarrow$ (0, 1)	(0, 0) $\rightarrow$ (1, 1)	(0, 3) $\rightarrow$ (9, 3)
$f_{SA}^{\text{exp}}$ (previous)	1 314 925 752.910(17)	58 605 052 164.24(86)	415 264 925 500.5(1.2)
$f_{SA}^{\text{exp}}$ ( $\eta = 1$ )	1 314 925 752.978(14)	58 605 052 164.14(16)	415 264 925 501.3(0.4)
$f_{SA}^{\text{exp}}$ ( $\eta = 3.56$ )	1 314 925 752.978(48)	58 605 052 164.14(55)	415 264 925 501.3(1.6)
$f_{SA}^{\text{exp}}$ ( $\eta = 3.56$ and corr. ind. unc.)	1 314 925 752.978(48)	58 605 052 164.14(56)	415 264 925 501.3(1.6)

TABLE V. Spin-averaged transition frequencies (in kHz). Previous determinations from the original publications [23–25] are given in the first line. The results of the least-squares adjustment performed in the present work are given in line 2. These results were obtained with an expansion factor  $\eta = 1$  (i.e. no expansion factor applied). The spin-averaged frequencies in line 3 are obtained by applying an expansion factor  $\eta = 3.56$  to the uncertainties of all (experimental and theoretical) input data. Finally, line 4 shows the frequencies for  $\eta = 3.56$  and including the hyperfine-correlation-induced uncertainty, which are added to the uncertainty of the adjustment in quadrature. These frequencies are our recommended values.

Label	Input datum	Value	Rel. Uncertainty	Reference
A1	$f_{SA}^{\text{exp}}[(0,0) \rightarrow (0,1)]$	1 314 925 752.978(48) kHz	$3.7 \times 10^{-11}$	this work
A2	$f_{SA}^{\text{exp}}[(0,0) \rightarrow (1,1)]$	58 605 052 164.14(56) kHz	$9.6 \times 10^{-12}$	this work
A3	$f_{SA}^{\text{exp}}[(0,3) \rightarrow (9,3)]$	415 264 925 501.3(1.6) kHz	$3.9 \times 10^{-12}$	this work
B1	$\delta E(0, 0)$	0.0000(21.2847) kHz		[28]
B2	$\delta E(0, 1)$	0.0000(21.2660) kHz		[28]
B3	$\delta E(1, 1)$	0.0000(20.7987) kHz		[28]
B4	$\delta E(0, 3)$	0.0000(21.1740) kHz		[28]
B5	$\delta E(9, 3)$	0.0000(18.1780) kHz		[28]
C1	$m_e$ (CODATA 2018)	$5.485\,799\,090\,65(16) \times 10^{-4}$ u	$2.9 \times 10^{-11}$	[1]
C2	$m_d$ (AMDC 2020)	2.013 553 212 537(15) u	$7.5 \times 10^{-12}$	[44]
C3	$m_p$ (AMDC 2020)	1.007 276 466 587(14) u	$1.4 \times 10^{-11}$	[44]
C4	$m_d/m_p$ (Fink 2021)	1.999 007 501 272(9)	$4.5 \times 10^{-12}$	[7]
C5	$cR_\infty$ (CODATA 2018)	3 289 841 960 250.8(6.4) kHz	$1.9 \times 10^{-12}$	[1]
C6	$r_p$ (CODATA 2018)	0.8414(19) fm	$2.2 \times 10^{-3}$	[1]
C7	$r_d$ (CODATA 2018)	2.12799(74) fm	$3.5 \times 10^{-4}$	[1]

TABLE VI. Input data for the adjustments discussed in Sec. V.

Correlation coefficients					
$r(A1, A2) = 0.00036$	$r(A1, A3) = 0.00644$	$r(A2, A3) = 0.00741$	$r(B1, B2) = 1.00000$	$r(B1, B3) = 0.99999$	
$r(B1, B4) = 1.00000$	$r(B1, B5) = 0.99795$	$r(B2, B3) = 0.99999$	$r(B2, B4) = 1.00000$	$r(B2, B5) = 0.99795$	
$r(B3, B4) = 0.99999$	$r(B3, B5) = 0.99819$	$r(B4, B5) = 0.99798$	$r(C1, C5) = 0.00704$	$r(C1, C6) = -0.00133$	
$r(C1, C7) = 0.00317$	$r(C2, C3) = 0.31986$	$r(C5, C6) = 0.88592$	$r(C5, C7) = 0.90366$	$r(C6, C7) = 0.99165$	

TABLE VII. Values of all nonzero correlation coefficients in the input data.

Transition	$f_{SA}^{\text{theor}}$ (kHz)	$\beta_{m_e}$	$\beta_{m_p}$	$\beta_{m_d}$	$\beta_{cR_\infty}$	$\beta_{r_p}$	$\beta_{r_d}$
(0, 0) $\rightarrow$ (0, 1)	1 314 925 752.929(19)	2.3653[+12]	-8.5857[+08]	-2.1492[+08]	3.9969[-04]	-1.5312	-3.8742
(0, 0) $\rightarrow$ (1, 1)	58 605 052 163.88(49)	5.1767[+13]	-1.8790[+10]	-4.7036[+09]	1.7814[-02]	-40.813	-103.12
(0, 3) $\rightarrow$ (9, 3)	415 264 925 502.7(3.2)	2.6664[+14]	-9.6785[+10]	-2.4227[+10]	1.2623[-01]	-268.24	-674.83

TABLE VIII. Theoretical values and sensitivity coefficients of HD<sup>+</sup> transition frequencies. Theoretical frequencies are calculated using 2018 CODATA values of  $m_e$ ,  $m_p$ ,  $m_d$ ,  $cR_\infty$ ,  $r_p$ ,  $r_d$ , and  $\alpha$ . Their theoretical uncertainties (which do not include uncertainties from the fundamental constants) are indicated between parentheses, and are computed from input data B1–B5 (Table VI) in combination with the correlation coefficients of Table VII. Sensitivities to particle masses ( $\beta_{m_e}$ ,  $\beta_{m_p}$ ,  $\beta_{m_d}$ ) are given in kHz.u<sup>-1</sup>. The sensitivity to the Rydberg constant  $\beta_{cR_\infty}$  is dimensionless, and sensitivities to nuclear radii are given in kHz.fm<sup>-1</sup>.

Adjustment	Input data	$m_p/m_e$	$u_r$ ( $10^{-11}$ )
1	C1-C4	1 836.152 673 353(56)	3.0
2	A,B,C1-C2,C5-C7	1 836.152 673 514(66)	3.6
3	All	1 836.152 673 423(33)	1.8

TABLE IX. Adjustment results.

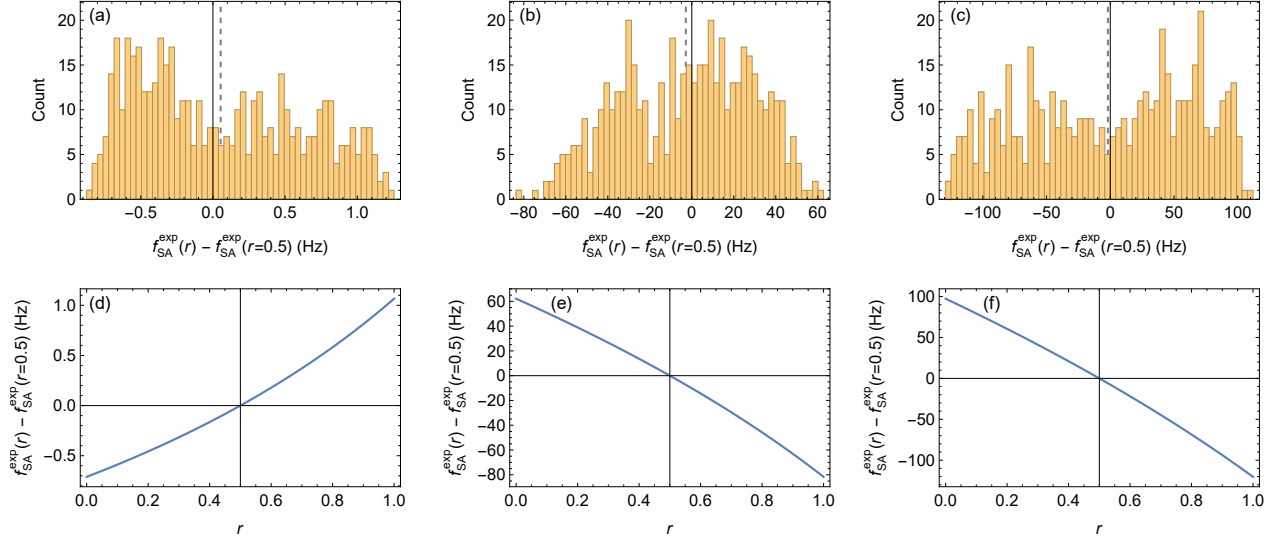


FIG. A1. Distribution of correlation-induced shifts of spin-averaged frequencies obtained from a Monte-Carlo simulation consisting of 502 runs. Here the argument  $r$  represents the vector  $(r_1, r_2, r_6, r_8, r_9)$ ; likewise  $r = 0.5$  stands for the vector  $(0.5, 0.5, 0.5, 0.5, 0.5)$  (a) Distribution for the  $(v, L): (0, 0) \rightarrow (0, 1)$  transition. (b) Distribution for the  $(v, L): (0, 0) \rightarrow (1, 1)$  transition. (c) Distribution for the  $(v, L): (0, 3) \rightarrow (9, 3)$  transition. Dashed vertical lines indicate the mean value of the frequency distribution. (d) Frequency shift of the  $(v, L): (0, 0) \rightarrow (0, 1)$  transition if all components of the vector  $r$  are varied simultaneously. (e) Same as (d), but for the  $(v, L): (0, 0) \rightarrow (1, 1)$  transition. (f) Same as (d), but for the  $(v, L): (0, 3) \rightarrow (9, 3)$  transition. .